2018 IEEE International Conference on Robotics and Automation (ICRA)
May 21-25, 2018, Brisbane, Australia

Development and Implementation of High Power Hexapole Magnetic Tweezer System for Micromanipulations

Xiao Zhang, Hoyeon Kim, Louis W. Rogowski, Samuel Sheckman, and Min Jun Kim, *Member, IEEE*

Abstract— **This paper presents the design, development and implementation of a novel, high power hexapole magnetic tweezer system for 3D micromanipulations. Six tapering-tipped magnetic poles are deployed in a tilted Cartesian coordinate system, with an electromagnetic coil on each for actuation, connected by two 3D printed magnetic yokes to form a double layer structure. The power source is integrated to the magnetic tweezer system through a control algorithm on the software level; image processing was used for experiment analysis. Because of the high magnetic field that the magnetic coils can generate, the working space in the system is relatively larger than other similar designs, which provides better performance on microscale robotic swimmer manipulations. Simulations and experiments performed in this paper demonstrate the agile and powerful manipulation of microswimmers with desired control input to follow complex trajectories, avoid obstacles and move against micro-flow in the samples. We prove that the developed hexapole magnetic tweezer has enough power and controllability to guide microswimmers in Newtonian and Non-Newtonian fluid environments. The system will be optimized continuously and implemented into cell penetration experiments. Finally, the application will be deployed into *in vivo* based environments.**

I. Introduction

Micromanipulation via a magnetic tweezer system is a straightforward methodology. Applications can be simplified as using magnetic coils to generate a magnetic field gradient around a magnetic pole; this applies force directly onto magnetized objects within the working area. As compared in [1], [2], magnetic tweezer systems have advantages that make it preeminent among all other tools, such as AFM, electromagnetic coil systems and optical tweezers. It can generate multi-direction and non-contacting force, therefore not requiring the microswimmer to have nonreciprocal motion for swimming in low Reynolds number environments [3]. Magnetic force will only be applied to objects that are magnetized designedly, so magnetic tweezers are ideal for *in vivo* applications, as most biological materials are free from magnetic influence [4-7]. Tapering-tipped magnetic poles, with high magnetic permeability properties, are necessary to allow the magnetic flux generated from the magnetic coils to be released to the surroundings efficiently. This generates high magnetic field gradient; however, magnetic field strength decreases quickly on areas far away from the pole tip, which introduce the magnetic force into the working space [8-10]. To generate multiple degrees of freedom forces, multiple magnetic poles are placed in different pointing directions as each pole can only apply a single direction attractive force. Six pole structures with three poles on each of the top and bottom plane are necessary for 3D control [6]. Microrobotics has a highly promising future in medical-related applications [11], such as drug delivery and minimally invasive surgery. Former researches [4], [5], [8], [12-16] have demonstrated that magnetic tweezer system has the capability to generate versatile and powerful force to satisfy these application requirements. However, the magnetic tweezer system in this paper provides better performance than earlier adaptations used in previous research. On the power level, each of the coil has 527 turns and can provide up to 630 Ampere-turn to generate the magnetic field. The effective working space from simulation results and experimental experience, is about 2.5 mm × 2.5 mm on *xy* plane and 0.5 mm on *z* direction, enabling experimentation with larger groups of microswimmers. The six magnetic poles are aligned naturally on a tilted Cartesian coordinate system, the further computation for rotation between actuation and measurement coordinates is also simplified [8], [14-16]. 3D printing technology was critical for this system designs as it allows us to fabricate the hexagonal magnetic yokes with ferromagnetic material; as such, the yokes are lighter and easier to machine, while still maintain strong magnetic properties. Magnetic tweezer systems utilize force mechanisms, differing from past microswimmer control that applies magnetic torque strategies. However, it does not require either chirality (helical structure swimmers, etc.) or flexibility (such as sperm-like swimmers) properties to generate propulsion under rotating magnetic field [17]. In this paper, we mainly used single bead microswimmers for experimentation and analysis. The compendium of the paper is as follows. Section II illustrates the magnetic tweezer system setup and controlling algorithm specifications. Section III shows the simulation result under different current configurations on the poles. Section IV introduces various motion control experiment data and analysis. The conclusion is in Section V.

II. Design of Magnetic Tweezer System

A. Magnetic Tweezer System Hardware Integration

The CAD model and coordinate systems of the hexapole magnetic tweezer system are illustrated in Fig. 1. To achieve the high efficiency and power output, high magnetic permeability and magnetic saturation material are essential for defining the poles.

VACOFLUX 50 (Cobalt Iron Alloy) was chosen as the pole material as its high saturation (2 T) feature and the material machinability for cutting the sharp-tipped pole shape, was proved optimal. Heat generation caused by the

Xiao Zhang, Hoyeon Kim, Louis W. Rogowski, Samuel Sheckman and Min Jun Kim are with the Department of Mechanical Engineering, Southern Methodist University, Dallas, TX 75275, U.S.A. (email: mjkim@lyle.smu.edu).

978-1-5386-3081-5/18/$31.00 ©2018 IEEE

hysteresis effect is expected to appear if the magnetic field changes frequently. However, through the temperature analysis later in this section, and actual performance during the experiments in the other sections, it shows that the applied current fulfills our demand and natural convection is more than satisfactory [16]. Sharp-tipped pole shapes were laser cut by Polaris Laser Laminations, LLC for the overall shape, further improvement of the pole tips was perfected by individually machining. The final dimension of the tip radius is about 40 µm, which has been shown earlier in [1]. The tip shape uniformity is very easy to be broken due to the extremely small dimension and machining resolution limitations. Six magnetic poles align in pairs on top and bottom yokes to form an inclined Cartesian coordinate system, which is called the actuation coordinate system. The angle between each pair of poles and the plane is 35.26°. Six magnetic coils are positioned on the two yokes at the end of each pole, the central sample disk is installed on the

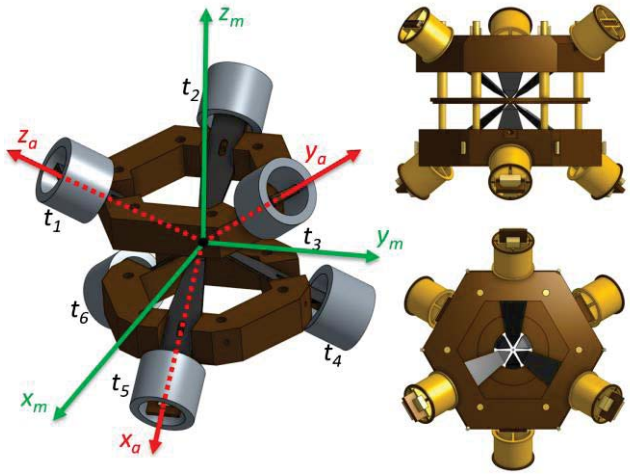

Fig. 1. Magnetic tweezer CAD model and coordinate systems.

microscope platform to connect and support the entire system on an Olympus IX50 inverted system microscope. A color camera (EO-3112C ½" CMOS) using 15 FPS and an Olympus 40× objective are mounted on the microscope for image capturing and processing. The novel hexagonal magnetic yokes were 3D printed with magnetic material to form a closed magnetic circuit in the system; while improving the efficiency of the magnetic field flux generation and reducing the exciting current necessary for generating magnetic field gradient[16]; this also helped reduce heating issues. . The magnetic coils are wounded of AWG 25 copper wire with heavy-built insulation coating, and 527 turns for each. Three power supplies (GW Instek Programmable Digital AC/DC Power Supply) were connected to three Relays (AXICOM D3023), respectively. Each relay connects one pair of coils to the National Instrument SCB-68A Connector Block, which communicates with our customized control interface through a National Instrument PCIe 6323 board, to generate magnetic field in different directions. Fig. 2 illustrates the setup system connections. After eliminating the production and position error during the installation process, each pole on the same plane has a gap of 3.668 mm, the distance between top and bottom planes are 2.040 mm. Through simulation results and experimental experience, the effective working space is about 2.5 mm × 2.5 mm × 0.5 mm. A polydimethylsiloxane (PDMS) chamber with a 2 mm × 2 mm sink is then used in the center of the central sample disk to contain the solution samples for experimentation. Microbeads with average diameters of 4.21

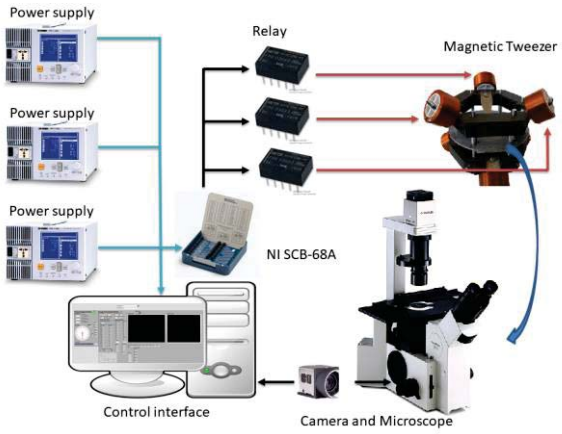

Fig. 2. Magnetic tweezer system scheme.

µm were mixed with 20% NaCl or 0.5% synthetic mucus to get 1% concentration sample for different experiments. The sample are then vortexed for 30 seconds and magnetized by approaching to a permanent magnet for 15 seconds before injecting into the PDMS chamber.

B. Magnetic Tweezer System Software Illustration

The customized control interface is based on LabVIEW and MATLAB with 3rd party drivers provided by camera and power supply manufacturers. The control algorithm consists of three parts: power supply control, camera control and image processing. Power supply control operates three power supplies depending on the control inputs from the user, the relays redirect current direction into the different coils for each pair; this depends on the negative or positive sign of the power input vector. Camera control configures image capture specifications, such as balancing exposure time with frame rate and resolution. Normally high resolution and exposure time will set limitations on the frame rate. Experimental video

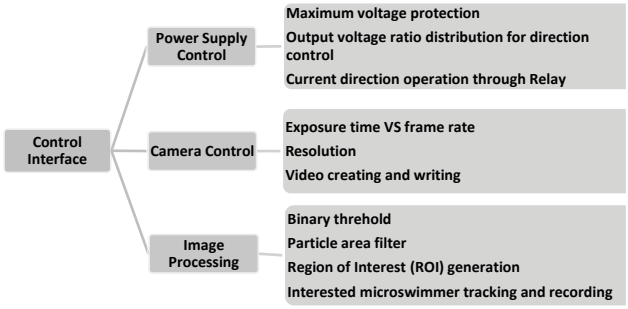

Fig. 3. Function of control interface

writing and saving is also functionalized. Image processing allows the user to adjust different parameters, so necessary information including object trajectory, time and so on can be distinguished and recorded during the experiment. Videos are then saved after all processes are complete for post-experimental analysis. The control strategy contains

coordinate transformation, normalizing space vector and then amplifying power output. A minimal number of three different direction orthogonal forces are necessary for 3D control. The tilted actuation and rotated measurement coordinate systems are shown in Fig. 1. All 6 poles in the actuation coordinate system are located at the face centers of a face centered cubic [15] and form two inclined planes, tips 1-3 are aligned on the top plane and tips 4-6 are on the bottom plane. After a two-step coordinate system rotation, it can be related with the measurement coordinate system [8], [15]. The rotation transformation is derived from rotations of y axis and x axis as explained in Eq. (1) and Fig. 1.

$$ {}^{a}_{m}R = [R_x(45^\circ)][R_y(35.26^\circ)] = \begin{bmatrix} 0.8165 & 0 & -0.5774 \\ 0.4082 & 0.7071 & 0.5774 \\ 0.4082 & -0.7071 & 0.5774 \end{bmatrix} \quad (1) $$

Once the direction input is given on the user interface; the force direction vector will be transformed into the actuation coordinate system and then converted into a power supply output ratio. Power supplies will change the output instantly to relays and further change current in each coil, which will achieve desired motion in measurement coordinate system. The force generated from single pole on a single bead can be expressed as [15], [18]:

$$ \boldsymbol{F} = (\boldsymbol{m} \cdot \boldsymbol{\nabla})\boldsymbol{B} \quad (2) $$

$$ \boldsymbol{m} = \frac{\pi d^3}{2\mu_0}\left(\frac{\mu-\mu_0}{\mu+2\mu_0}\right)\boldsymbol{B} \quad (3) $$

where $\boldsymbol{m}$ is the magnetic moment of the microswimmer, a combination of more microbeads in microswimmer means a stronger magnetic moment. $\boldsymbol{B}$ is the magnetic flux density, μ is the permeability of microswimmer, μ_0 is the permeability of free space, d is the diameter of microbead. For distances far from the tips, the overall force can be simplified as a superposition of all the force vectors. As the magnetic force generated is directionally related to both magnetic field gradient and magnetic moment of the microswimmer, in order to get a stronger force generation, it is feasible to either increase the power output or choose microswimmers with larger particle aggregations

The relationship between temperature and current on different parts of magnetic tweezer system are shown in Fig. 4. The results are recorded with a time scale of 10 minutes with different current inputs, which are the regular time length for our experiment. Coil temperature increases quickly under high current while the temperatures in magnetic poles and sample chamber are negligible. Under this situation, the system does not need an extra cooling method as natural heat dissipation is quite enough for the experiment purpose.

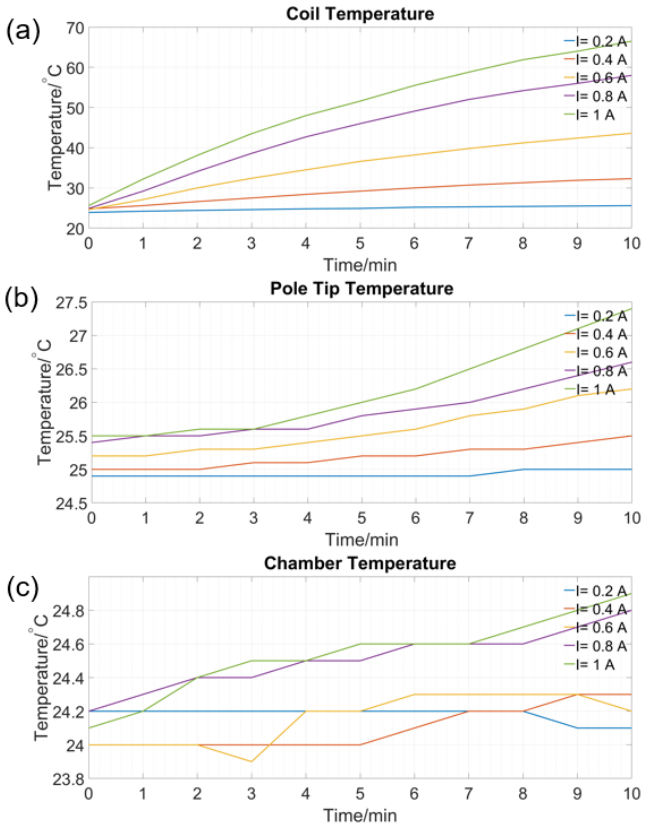

Fig. 4. Temperature increase under different currents on each part of magnetic tweezer system.

III. Simulation

The simulation was done using COMSOL Multiphysics to analyze the magnetic field production with the actuations of single or multiple coils. The CAD models are pre-built in

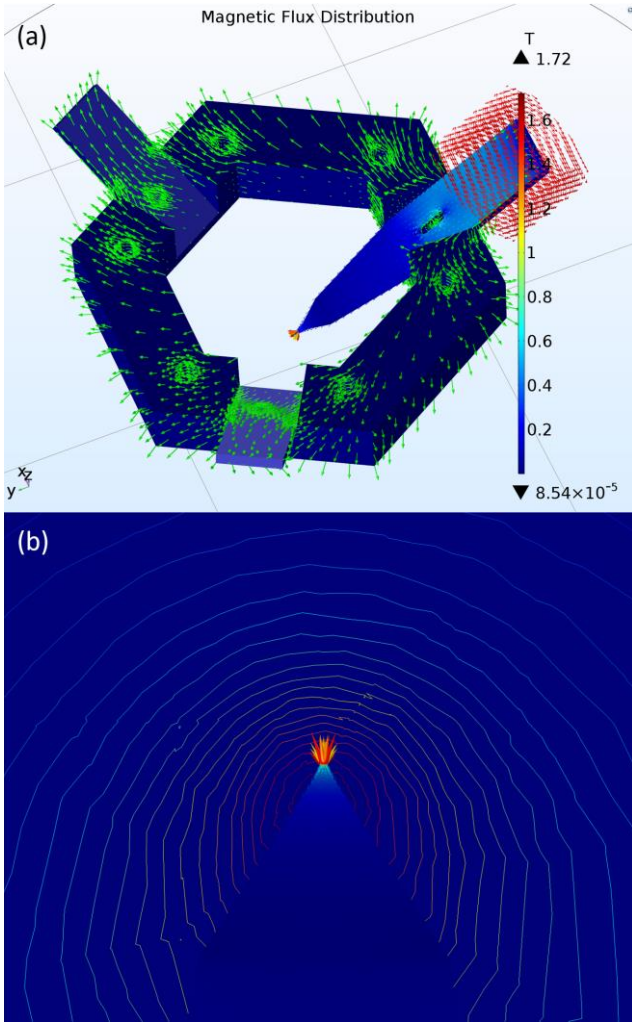

Fig. 5. (a) Magnetic flux direction distribution of tweezer system under single coil actuation. (b) Magnetic field strength near the pole.

Onshape and then imported into COMSOL for meshing and computation operations. Current with a clockwise direction applied in single coil analysis was constant at 1 Ampere and has different ratios in multiple coil analysis so that all the magnetic fields generated will point toward the working space.

Fig. 5 shows the simulation results of magnetic flux distribution on single magnetic coil, yoke and pole. In Fig. 5(a), it is obvious that the uniform magnetic field generated from the coil transmits into the pole and then drastically released at the sharp tip. There are negligible leakages at corners of the yoke and middle area of the pole, which is also due to the relatively sharp extrusions. The maximum magnetic strength at the sharp tip under 1 A can be as high as 1.72 T and decreases rapidly with the distance increasing from the pole, which can be seen in the magnetic field strength distribution on the working plane in Fig. 5(b).

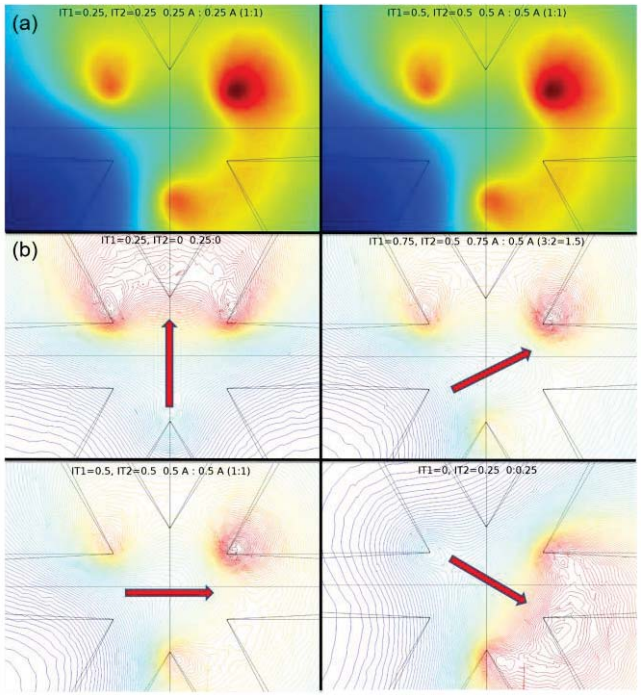

Fig. 6. (a) Magnetic field comparsion under same current ratio. (b) Magnetic field comparsion under different current ratios.

The result presented in Fig. 6(a) shows the magnetic field distribution under different currents. IT1 is the current on top pole and IT2 is the one on right pole. These show that the distribution maintains the same within the working space, if the current ratio remains constant. Thus, helping to construct the control algorithm to manipulate microswimmer performing same movement with different forces and velocities. Fig. 6(b) illustrates the superimposed magnetic gradient directions under different current input ratios. As ratio increases to the right pole, the working space magnetic field direction is gradually moving clockwise, and ultimately pointing to it when there is only current applied in that single pole. With different current input combinations, the gradient output direction will also show appropriate changes. As mentioned in [1], the velocity is directly related to input current. For constant direction movement, higher power input will improve microswimmer's capability for overcoming external disturbance and achieve faster operations.

IV. Motion Control Validation

In order to measure the control flexibility, such as microswimmer force output and 3D motion; we introduced single bead and multi-bead microswimmers into NaCl solution and synthetic mucus samples. Both samples act as mechanism to check the control algorithm capability and microswimmer performance when placed in different medium. The directional control matches accurately with the microswimmer heading direction with instant response. In 3D motion testing, SU-8 structure from microfabrication are deployed on the bottom of the sample. When the magnetic field varies in the working space, as the material is non-magnetized, the obstacles will remain still on the bottom. Thus, distinguishing if the microswimmers are moving against the gravity force and the direction the microswimmers are moving out of the horizontal plane.

A. Control Flexibility and Obstacle Avoidance

By operating the control interface to manipulate a single bead microswimmer, beads could be manipulated to follow complex trajectories. In this case, we used it to spell out the initials of our laboratory. Once completed, the results were stitched together via image processing. The 'SMU BAST' lab trajectories are shown in Fig. 7. The currents vary in range on the three power supplies between 0 A- 1.2 A, limited by the voltage protection preset in control algorithm to protect the system. During experimentation, microswimmers move agilely while external disturbance like microflow and foreign substance exists. Each trajectory was finished within 50 s with high accuracy rate. Further development will be accomplished to introduce advanced control in the magnetic tweezer system to elevate the accuracy, power efficiency and other performances [14].

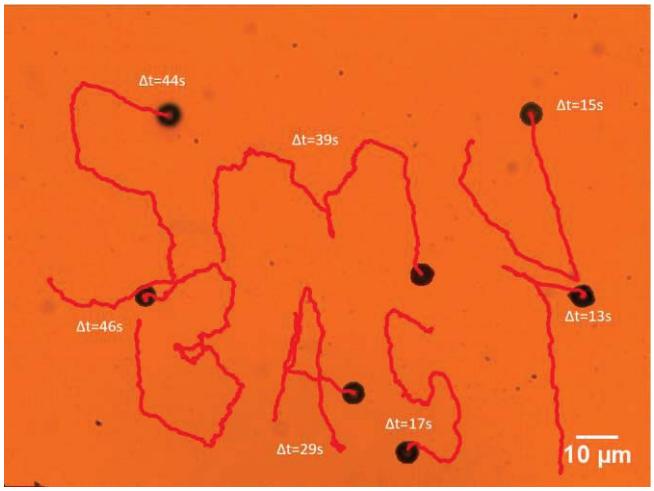

Fig. 7. SMU BAST lab trajectory This is the same bead completing multiple trajectories which were then superimposed into a single image.

Mucus, primarily composed of mucin glycoproteins, DNA, lipids, salts, cells, and cellular debris, exists throughout a living animal's body, with very distinct viscos-elastic properties. Mucin is the primary component of mucus responsible for non-Newtonian effects [19]. The viscosity in synthetic mucus is different as location varies and there are a lot of bulk particles existing in the flow, which provide excellent conditions for simulating *in vivo* environments [20],

[21]. A solution of 0.5% synthetic mucus, a non-Newtonian fluid, is also used for demonstrating obstacle avoidance. From Fig.8(a), we manipulated a two-bead microswimmer, which produced a larger magnetic moment generating a stronger magnetic force, when compared to single bead microswimmers. In comparison to the 20% NaCl solution from Fig. 7, it is obvious that the traveling time for the relative path length in synthetic mucus was still higher. This is mainly caused by the high and randomly varying viscosities and bulk substances. When the microswimmer became immobile due to the high viscosity or microstructures inside the flow, we rotated the controllable magnetic field direction, while increasing the power input to make the microswimmer suddenly 'jump' or crawl (Left side of Fig. 8(a) and Fig. 8(b), the microswimmer performed crawling several times shown as the trajectory direction changing drastically and high velocity with distinctive deviations). Thus, the microswimmer will escape from that area and then continue the task with more stable speed. The two-bead microswimmer traveled freely within the working area with a relatively slow speed about 4 μm/s. Still, it is certain that with a higher power input and more optimal control strategy, the speed performance will substantially improve.

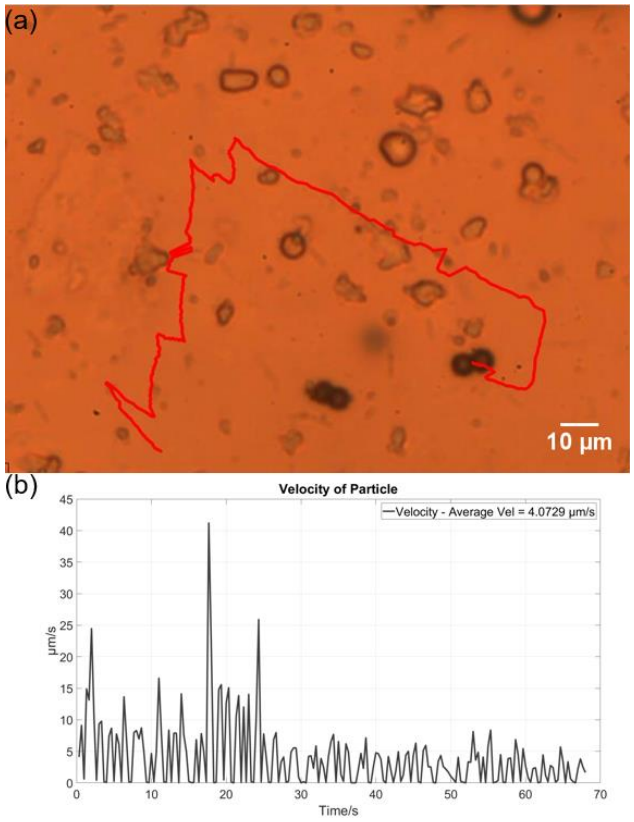

Fig. 8. (a) Controlled microswimmer moving from bottom left to top first and then moving toward bottom right to avoid bulk particles in synthetic mucus. (b) velocity analysis in (a).

B. Magnetic Force against Microflow

Presence of microflows are a very important issue in microswimmer applications that needs to be addressed, as microflows exist everywhere in the *in vivo* environments. It is noteworthy that swimming within microflows under controllable maneuverability is a challenge that researchers need to overcome for further *in vivo* applications. In Fig. 9, the three-bead microswimmer first freely drift downward without any control input from the top following the microflow in the chamber, which is indicted as the vertical black trajectory on

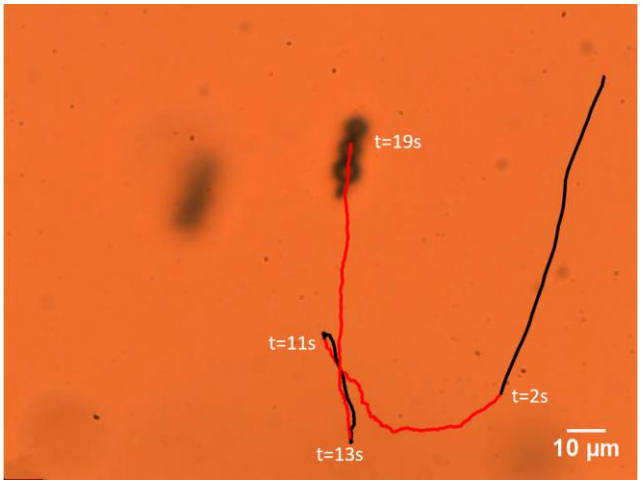

Fig. 9. microswimmer trajectory in sample with microflow inside. Black part is swimming with microflow and red part is swimming against microflow under control input.

the right. After 2 s, the control starts to get involved, giving a direction control to the upper left with an increasing power input, which is shown as the curved red trajectory on the bottom. The microswimmer first maintains its motion downward, while also starts to move to the left. As power increases, the moving direction changes gradually and then finally reversed. At 11 s, the control input is turned off and the microswimmer drifts for 2 s before the control input is turned back on again at 13 s, this is shown as the vertical short black and red trajectories on the bottom. The microswimmer continues to move upward against the micro flow for another 6 s. By comparing the microswimmer performance with/without control input, it's easy to find that the force generation provides enough power to actuate the microswimmer in complicated environment.

C. 3D Motion Testing

3D motion of microswimmers present more capabilities to complete versatile tasks in practical applications, in both *in vitro* and *in vivo* environments. The current 3D motion phenomena achieved by the magnetic tweezer system can be distinguished indirectly. SU-8 microstructures of uniform diameter of 10 μm, are imported into sample and sink onto the bottom as reference for z axis direction recognition. When adjusting the microscope focal plane away from the objects, the pattern will get blurred and the size will increase [19]. In Fig. 10, at t = 0 s, single bead microswimmers sunk on the bottom of the glass substrate with the other obstacles. Several direction control vector inputs that including positive z direction control were then configured one by one, to control the microswimmer roaming. As the experiment continued, the microswimmer moved away from the original focal plane. As we kept adjusting the microscope to focus on the microswimmer, the blurred background and increased SU-8 substance size indicate that microswimmer has 3D motion.

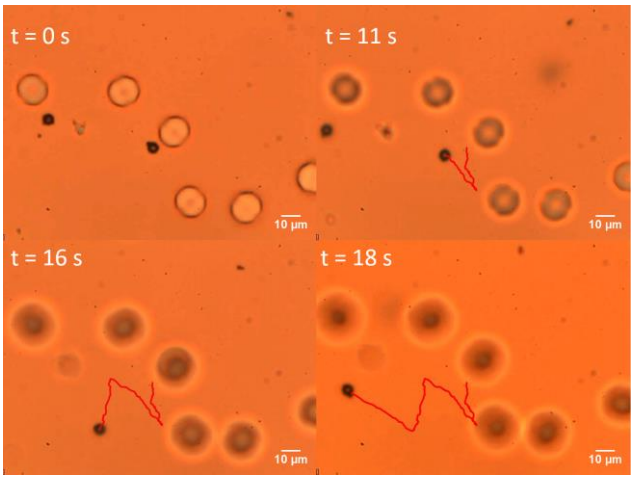

Fig. 10. 3D motion task with SU-8 comparison obstacles As time increases, the background structures come out of focus with the objective; this signifies the particle is swimming upward.

Thus, overcoming its own gravity force to move upward.

V. Conclusion

In conclusion, this paper illustrated the design, mechanics, implementation, and testing of a hexagonal 3D magnetic tweezer system. Various experiments with different purposes were completed; the controllability and force generation capability of microswimmer manipulation with multiple directional magnetic forces present was demonstrated, in Newtonian and non-Newtonian fluid environments. The analysis of temperature effect on the system was achieved. Single and multi-bead microswimmers performing desired trajectories, obstacle avoidance in non-Newtonian microflow under the magnetic force were performed. Force generation capability is shown through the phenomena of resisting microflow back and forth in the sample. 3D motion is also observed through focal plane comparison. The magnetic tweezer system established in this paper outstrips other configurations, as the working space is significantly larger, operated at a higher power output and shown novel applications. The force superposition approach worked effectively as an approximation within the working space, where the magnetic field gradient distribution maintains uniform. Microswimmer formed of higher threads of microbeads generate higher magnetic force together with the magnetic tweezer system. Changing both the power input and microswimmer size can help achieve various manipulation performances. Feedback control and 3D motion tracking and analysis algorithm will be developed.

Acknowledgment

This work was supported by the National Science Foundation (CMMI 1737682). Special acknowledgement to Professor U Kei Cheang at Southern University of Science and Technology for his strong support and valuable instructions during experimental setup.

References

1. Zhang, X., H. Kim, L.W. Rogowski, S. Sheckman, and M.J. Kim. *Novel 3D magnetic tweezer system for microswimmer manipulations*. in *Ubiquitous Robots and Ambient Intelligence (URAI), 2017 14th International Conference on*. 2017. IEEE.
2. Neuman, K.C. and A. Nagy, *Single-molecule force spectroscopy: optical tweezers, magnetic tweezers and atomic force microscopy.* Nature methods, 2008. **5**(6): p. 491-505.
3. Purcell, E.M., *Life at low Reynolds number.* American journal of physics, 1977. **45**(1): p. 3-11.
4. Zhang, Z., K. Huang, and C.-H. Menq, *Design, implementation, and force modeling of quadrupole magnetic tweezers.* IEEE/ASME Transactions on Mechatronics, 2010. **15**(5): p. 704-713.
5. Matsuura, D., H. Aoki, and Y. Takeda. *Development of a 3D-magnetic tweezer system having magnetic pole positioning mechanism*. in *Robotics and Automation (ICRA), 2016 IEEE International Conference on*. 2016. IEEE.
6. Bausch, A.R., W. Möller, and E. Sackmann, *Measurement of local viscoelasticity and forces in living cells by magnetic tweezers.* Biophysical journal, 1999. **76**(1): p. 573-579.
7. Haber, C. and D. Wirtz, *Magnetic tweezers for DNA micromanipulation.* Review of Scientific Instruments, 2000. **71**(12): p. 4561-4570.
8. Zhang, Z. and C.-H. Menq, *Design and modeling of a 3-D magnetic actuator for magnetic microbead manipulation.* IEEE/ASME Transactions on Mechatronics, 2011. **16**(3): p. 421-430.
9. Amblard, F., B. Yurke, A. Pargellis, and S. Leibler, *A magnetic manipulator for studying local rheology and micromechanical properties of biological systems.* Review of Scientific Instruments, 1996. **67**(3): p. 818-827.
10. Niu, F., W. Ma, X. Li, H.K. Chu, J. Yang, H. Ji, and D. Sun. *Modeling and development of a magnetically actuated system for micro-particle manipulation*. in *Nanotechnology (IEEE-NANO), 2014 IEEE 14th International Conference on*. 2014. IEEE.
11. Kei Cheang, U., K. Lee, A.A. Julius, and M.J. Kim, *Multiple-robot drug delivery strategy through coordinated teams of microswimmers.* Applied physics letters, 2014. **105**(8): p. 083705.
12. Chen, L., V. Maybeck, A. Offenhäusser, and H.-J. Krause, *Implementation and application of a novel 2D magnetic twisting cytometry based on multi-pole electromagnet.* Review of Scientific Instruments, 2016. **87**(6): p. 064301.
13. de Vries, A.H., B.E. Krenn, R. van Driel, and J.S. Kanger, *Micro magnetic tweezers for nanomanipulation inside live cells.* Biophysical journal, 2005. **88**(3): p. 2137-2144.
14. Chen, L., A. Offenhäusser, and H.-J. Krause, *Magnetic tweezers with high permeability electromagnets for fast actuation of magnetic beads.* Review of Scientific Instruments, 2015. **86**(4): p. 044701.
15. Fisher, J.K., J. Cribb, K.V. Desai, L. Vicci, B. Wilde, K. Keller, R.M. Taylor, J. Haase, K. Bloom, and E.T. O'Brien, *Thin-foil magnetic force system for high-numerical-aperture microscopy.* Review of Scientific Instruments, 2006. **77**(2): p. 023702.
16. Long, F., D. Matsuura, and C.-H. Menq, *Actively Controlled Hexapole Electromagnetic Actuating System Enabling 3-D Force Manipulation in Aqueous Solutions.* IEEE/ASME Transactions on Mechatronics, 2016. **21**(3): p. 1540-1551.
17. Cheang, U.K., H. Kim, D. Milutinović, J. Choi, L. Rogowski, and M.J. Kim. *Feedback control of three-bead achiral robotic microswimmers*. in *Ubiquitous Robots and Ambient Intelligence (URAI), 2015 12th International Conference on*. 2015. IEEE.
18. Boyer, T.H., *The force on a magnetic dipole.* American Journal of Physics, 1988. **56**(8): p. 688-692.
19. Wu, M., J.W. Roberts, and M. Buckley, *Three-dimensional fluorescent particle tracking at micron-scale using a single camera.* Experiments in Fluids, 2005. **38**(4): p. 461-465.
20. Rogowski, L.W., H. Kim, X. Zhang, S. Sheckman, D. Kim, and M.J. Kim. *Swimming in synthetic mucus*. in *Ubiquitous Robots and Ambient Intelligence (URAI), 2017 14th International Conference on*. 2017. IEEE.
21. Astarita, G. and G. Marrucci, *Principles of non-Newtonian fluid mechanics*. 1974: McGraw-Hill Companies.